Fract. Engng Mater. Struct. Vol. 14, No. 5, pp. 515–530, 1991
Printed in Great Britain. 

8756-758X/91 $3.00 + 0.00


# EFFECT OF PARTIAL-COVERAGE UPON THE FATIGUE FRACTURE BEHAVIOUR OF PEENED COMPONENTS

S. A. MEGUID

Engineering Mechanics and Design Laboratory, Department of Mechanical Engineering, University of Toronto, 5 King's College Road, Toronto, Ontario, Canada M5S 1A4

*(Received in final form 30 July 1990)*

**Abstract**—The achievement of full-coverage during the application of shot-peening to critical components represents a major concern in the aerospace and power generation industries. It has been accepted, for many years, that full-coverage of such components is needed to attain the beneficial fatigue-life effects of the treatment. It has also been proposed, by a number of industrialists, that partial-coverage may apparently shorten the fatigue-life of the component because of the presumed presence of tensile residual stresses in the uncovered areas. Three aspects of the investigation were accordingly examined. The first deals with the *accurate measurement of peening coverage* using a three-dimensional surface profilometer arrangement. The second deals with the development of fatigue crack growth data for fully- and partially-peened components using an instrumented rotating-bend fatigue rig. The third deals with monitoring the residual stress field associated with different peening-coverage using the dissection method. In order to highlight the effect of the treatment upon the fatigue behaviour of the tested components, both theoretical and experimental techniques were considered. In the theoretical work, three-dimensional finite element analysis of circumferentially cracked notched and un-notched cylindrical components was considered in the development of the corresponding stress-intensity factor ($K_I$) under bending loads. The stress-intensity factor vs crack length relationship was subsequently used in the experimental determination of fatigue crack growth rate data at the different stress levels examined. Accordingly, room temperature rotating-bend fatigue tests were conducted on specimens made from medium carbon steel 080 M40 (En 8) and aluminium alloy (7075-T6). Surprisingly, the results of both materials reveal that a life improvement of up to 50% can be attained at 35% coverage level.

## INTRODUCTION

Shot-peening is a cold-working process used mainly to improve the fatigue life and corrosion resistance of metallic components [1–3]. The results are accomplished by bombarding the surface of the component with small spherical shots made of hardened cast-steel, conditioned cut-wire, glass or ceramic beads at a relatively high velocity (70 m/s). After contact between the target and the shot has ceased, a small plastic indentation will have been made causing stretching of the top layers of the exposed surface. Upon unloading, the elastically stressed sub-surface layers tend to recover their original dimensions, but the continuity of the material in both zones, the elastic and the plastic, does not allow this to occur. Consequently, a compressive residual stress field followed by tensile will be trapped in the bounded solid. This surface compressive residual stress is highly effective in preventing premature failure under conditions of cyclic loading, since fatigue failure generally propagates from the upper most surface of the component, and usually starts in a region which is subjected to high tensile stresses.

Suppose in a peening process a target surface area ($A$) is exposed to a jet stream. Let the projected area produced by plastic indentation due to shot impingement be ($b$). It is interesting to note that if the number of shots impinging on the target surface is ($A/b$), the whole of the target surface area would not necessarily be covered by plastic indentations; some parts of the target would be struck by a shot more than once, and other parts would escape impingement altogether. The ratio

between the areas covered by the plastic indentations $S$ and the total exposed surface areas of the component $A$ is the coverage $C$. Complete or full-coverage means that $S = A$ and $C$ is therefore 100%.

It is worth noting that in certain circumstances, e.g. in the peening of very hard metals and very complex geometries, it is difficult not only to achieve but also to monitor full-coverage. The presence of un-peened areas in a peened component could represent a problem to the design especially if the implications of incomplete-coverage are not well understood. It is therefore paramount importance to examine the effect of partial-coverage upon the fatigue performance of metallic components.

Particular attention was therefore devoted to two related questions: (i) the influence of partial-coverage upon the resulting fatigue life and (ii) the influence of partial-coverage upon fatigue crack growth rate at the different stress levels examined.

Our objective was to evaluate whether partial-coverage is detrimental to the fatigue behaviour of the treated component. It was also desired to determine whether any life improvement can be achieved in cases where partial-peening treatment is unavoidable.

Extensive rotating-bending fatigue tests were carried out in order to determine the response of the materials tested to the above treatment. This experimental work was supplemented by coverage and crack growth measurements using a novel three-dimensional surface profilometer arrangement and a.c. potential-drop crack measurement equipment, respectively. This is detailed under the experimental analysis heading.

## THEORETICAL ANALYSIS

In order to obtain crack growth rate data from the fatigue/fracture experimental results, it was necessary to evaluate the stress intensity factor $K_I$ for V-notched circumferentially-cracked specimens subjected to remote uniform bending. Very few closed form solutions for three-dimensional cracked bodies exist in the literature; see for example Refs [4–7]. To overcome this difficulty, other techniques such as approximate analytical, numerical and experimental methods have been adopted in the determination of the stress intensity factor.

The theoretical work of the present investigation was based upon the three-dimensional finite element evaluation of the stress intensity factor $K_I$ for V-notched specimens, with a gauge length of 82 mm, average diameter ($2r_3$) of 24.6 mm and a reduced notch diameter ($2r_2$) of 15.25 mm, as depicted in Fig. 1. The displacement and stress results of the finite element analysis were utilized in the determination of $K_I$. Two methods were adopted; the first utilized the displacement field behind the crack tip as described by the following expressions

$$u = \frac{1+\nu}{4E}\sqrt{\left(\frac{2r}{\pi}\right)}\left(K_I\left[(5-8\nu)\cos\frac{\theta}{2}-\cos\frac{3\theta}{2}\right]+K_{II}\left[(9-8\nu)\sin\frac{\theta}{2}+\sin\frac{3\theta}{2}\right]\right)+0(r) \quad (1)$$

$$v = \frac{1+\nu}{4E}\sqrt{\left(\frac{2r}{\pi}\right)}\left(K_I\left[(7-8\nu)\sin\frac{\theta}{2}-\sin\frac{3\theta}{2}\right]+K_{II}\left[(3-8\nu)\cos\frac{\theta}{2}+\cos\frac{3\theta}{2}\right]\right)+0(r) \quad (2)$$

$$w = \frac{K_{III}}{\sqrt{2\pi r}}\cos\frac{\theta}{2}+0(r) \quad (3)$$

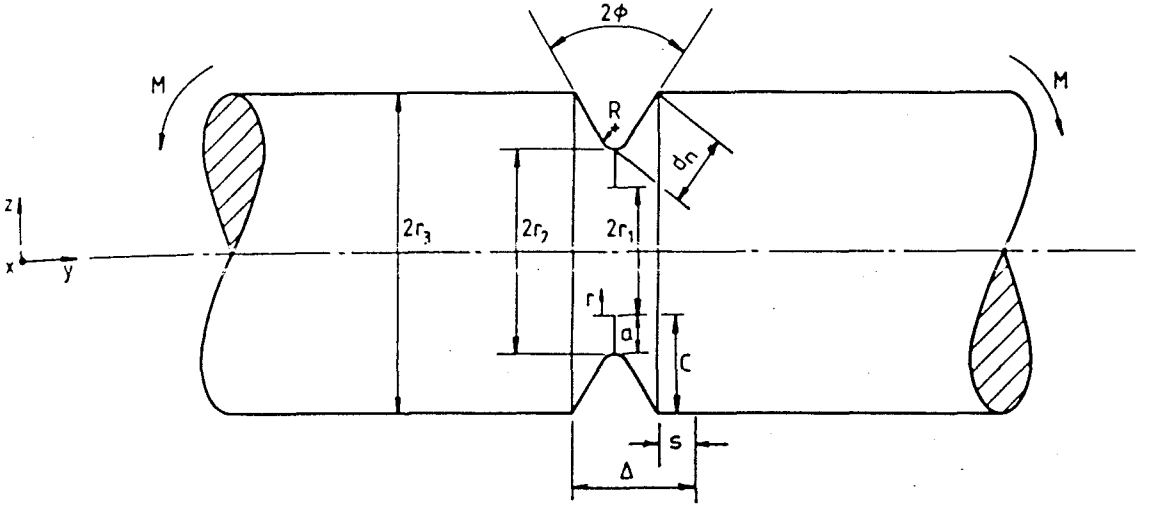


Fig. 1. Detailed geometry of specimen and notation used.

while the second utilized the stress field ahead of it, as described by the following equations

$$\sigma_x = \frac{K_I}{\sqrt{2\pi r}} \cos\frac{\theta}{2}\left[1 + \sin\frac{\theta}{2}\sin\frac{3\theta}{2}\right] - \frac{K_{II}}{\sqrt{2\pi r}} \sin\frac{\theta}{2}\left[2 + \cos\frac{\theta}{2}\cos\frac{3\theta}{2}\right] + 0(r) \tag{4}$$

$$\sigma_y = \frac{K_I}{\sqrt{2\pi r}} \cos\frac{\theta}{2}\left[1 + \sin\frac{\theta}{2}\sin\frac{3\theta}{2}\right] + \frac{K_{II}}{\sqrt{2\pi r}}\left[\sin\frac{\theta}{2}\cos\frac{\theta}{2}\cos\frac{3\theta}{2}\right] + 0(r) \tag{5}$$

$$\sigma_z = \nu(\sigma_x + \sigma_y) \tag{6}$$

where $E$ is Young's modulus, $\nu$ is Poisson's ratio and $K_I$, $K_{II}$ and $K_{III}$ are the conventional stress intensity factors [7, 8].

In view of the axisymmetric nature of the cracks generated by the current bending loads, the calculations of $K_I$ were based upon the following reduced forms of the displacement and stress fields

$$v = \frac{2(1-\nu^2)}{E}\sqrt{\frac{2r}{\pi}}K_I \tag{7}$$

and

$$\sigma_y = \frac{K_I}{\sqrt{2\pi r}}. \tag{8}$$

These calculations were performed in each of the considered cases, and by employing an extrapolation technique, it was possible to compute the appropriate stress-intensity factor $K_I$ at the crack-tip for circumferentially-cracked un-notched [FEM(A)] and notched [FEM(B)] specimens, as ... in Fig. 1. It is interesting to note that the accuracy of the finite element work was ex... odelling the effect of circumferentially cracked un-notched specimens upon the stress int... rs and comparing the results with the earlier analytical solutions of Benthem and Koiter [9] and Harris [10]. Figure 2 shows the outcome of the comparison and confirms that there exist a good agreement between the two. For a more detailed explanation of the 3-D finite element approach to this problem see Ref. [11].

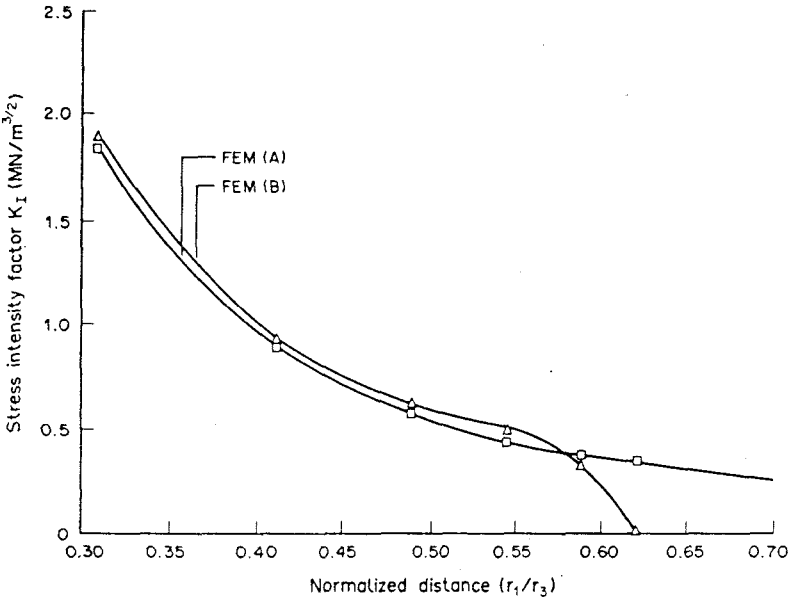


Fig. 2. Finite element results of the stress intensity factor $K_I$ vs normalized crack length for circumferentially-cracked un-notched [FEM(A)] and notched [FEM(B)] specimens.

## EXPERIMENTAL ANALYSIS

*Selection of materials and specimen design*

The experimental work was conducted on "target" materials made from medium carbon steel 080 M40 (En 8) and aluminium alloy (7075-T6) which are widely used in engineering applications. The mechanical properties of the En 8 steel used were: Young's modulus = 210 GPa, 0.2% proof stress = 530MPa, tensile strength = 850 MPa and Vickers hardness number of 348 at 500 $g_f$. The corresponding values for the 7075-T6 aluminium were 71 GPa, 410 MPa, 606 MPa and 209, respectively.

Preliminary tests were conducted on the steel and aluminium investigated in order to determine the specimen dimensions. The design requirement of the notch and overall dimensions of the specimens were dictated by the need to ensure: (i) elastic loading conditions, (ii) rigidity during dynamic loading, (iii) no distortion resulting from the peening treatment, and (iv) the number of grains existing across the reduced section was sufficient, so that the experimentally determined properties were representative of a polycrystalline material behaviour. As a compromise, it was decided to adopt the dimensions described earlier for both materials. The chemical composition of the medium carbon steel (wt%) as supplied by the manufacturer was as follows: 0.41 C, 0.23 Si, 0.027 P, 0.84 Mn, 0.03 S, remainder Fe, whilst that for the aluminium alloy 7075 was 5.98 Zn, 2.25 Mg, 1.28 Cu, 0.20 Cr, 0.19 Fe, 0.1 Si, 0.054 Ti, 0.05 Mn, 0.05 Zr, remainder aluminium. In order to minimize experimental scatter and improve repeatability a complete manual of the manufacturing procedure was laid down and guide-lines given in [12, 13] were followed whenever possible.

*Fatigue and crack measurement equipment*

The experimental programme conducted utilized an instrumented rotating-bend fatigue testing equipment. The uniform bending moment acting on the specimen was generated by loading

the appropriate arms with dead weights positioned at equal distances away from the specimen along the flexure shafts. Linear strain-gauge bridges were installed on one of the flexure shafts to facilitate both static and dynamic calibrations of the applied loads.

The crack detection and measuring equipment used was the "Crack Micro Gauge-Type U7G 300 Series", which is an a.c. field measuring equipment together with a 10 mm monitoring probe. Its principle of operation is based upon generating an a.c. field approximately normal to the defect plane under examination and measuring the potential drop between two electrodes of the probe. By comparing the potential drop at a non-defective area adjacent to the defect to that across the defect, a direct measure of the crack length $a$ may be determined.

In this work the following modified expression, which is based upon the earlier work of Dover [8], was used

$$d = r_3\left\{1 - \exp\left[-\left(\frac{V_c}{V_o} - \frac{S}{\Delta}\right)\frac{\Delta}{2r_3}\right]\right\} \tag{9}$$

where $V_c$ and $V_o$ are the voltages measured across the notch and adjacent to it, $d(d_n + a)$ is the depth of the crack, $r_3$ is the outer radius of the specimen, $\Delta$ is the probe-tip spacing and $S$ is the distance from the probe-tip to the edge of the notch, as shown in Fig. 1.

It is worth noting that the smallest crack depth measurable using this equipment is 0.05 mm and the largest depth is 45 mm. Post-mortem examinations were carried out to ensure that the crack depth is in agreement with what was actually measured by the above equipment.

### *Shot-peening treatment, coverage and residual stress measurement*

The shot-peening treatment was carried out on a specially modified direct-pressure automatically controlled air-peening system. The modifications included: (i) the introduction of three variable speed d.c. motors, thus enabling controlled linear and rotational movements during peening

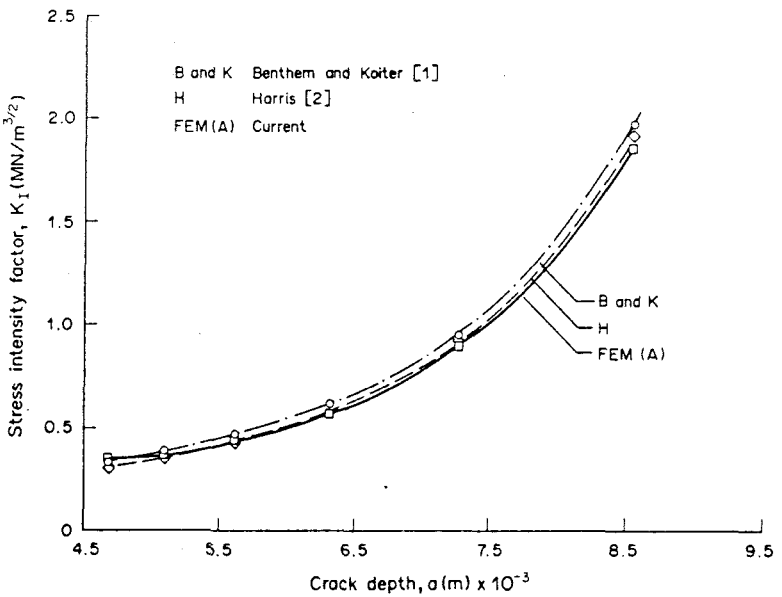


Fig. 3. Comparison between the current finite element results and the analytical solutions provided by Benthem and Koiter [9] and Harris [10] for circumferentially-cracked un-notched specimens.

Table 1. Details of peening parameters used in the study

| Peening parameters | Materials: Medium carbon steel En 8 | Aluminium alloy 7075 |
|---|---|---|
| Nozzle pressure (K Pa) | 172 | 70 |
| Mass flow rate (kg/min) | 1.2 | 0.4 |
| Shot material | Cast Steel | Glass |
| Shot-size | S170 | 400 800 $\mu$ |
| Shot hardness (HV) | 450 | — |
| Stand off distance (m) | 0.152 | 0.152 |
| Rotation of specimen holder (rev min) | 25 | 25 |
| Nozzle diameter (mm) | 7.5 | 7.5 |
| Jet obliquity | 90 | 90 |

applications, (ii) an improved separation system and (iii) an enhanced jet stream through an improved nozzle design and air circulation. This peening system was properly instrumented.

The choice of the peening parameters was based upon considerations of the specimen material and geometry as well as the desired peening coverages together with the guidelines set out in various standards, including the American Military Specifications (MIL-S-1316 B). Repeatability of the shot-peening process was achieved by rotating the specimens at a constant speed of 25 rev/min under the jet stream, which was in turn held constant by adjusting nozzle pressure and feed-valve setting.

The shot-size used was mainly determined by the root radius of the notch and the surface conditions of the specimen. The American Military Specifications "MIL-S-1316 B" on shot-peening recommend the use of shot diameter which is less than half of the notch root radius to be

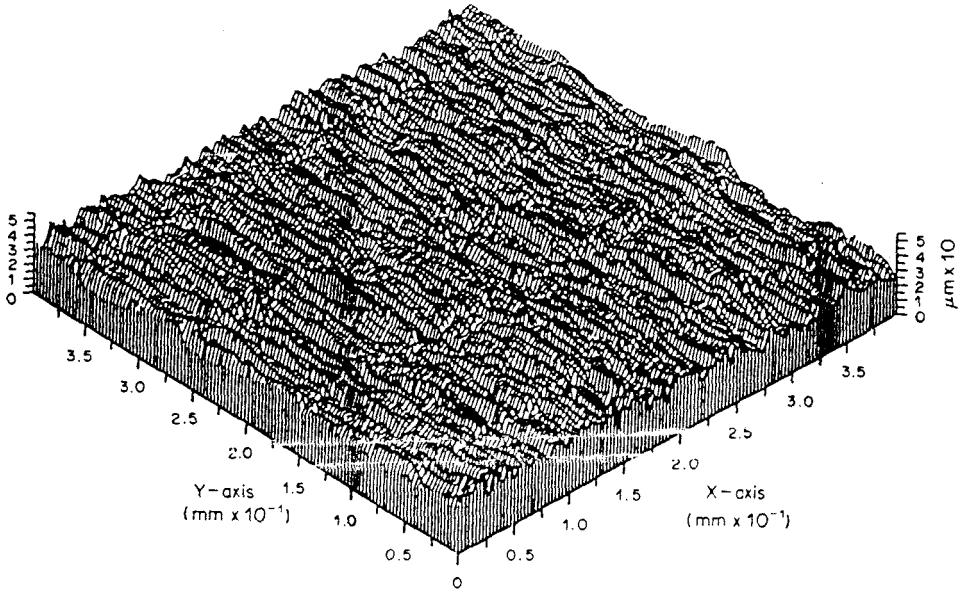


Fig. 4(a). *Caption on p. 524.*

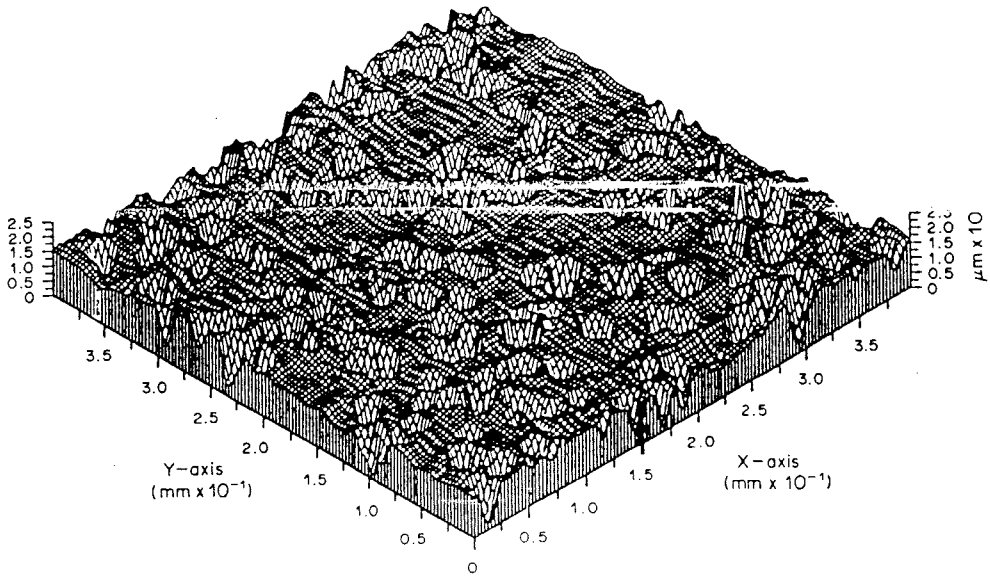


Fig. 4(b). *Caption on p. 524.*

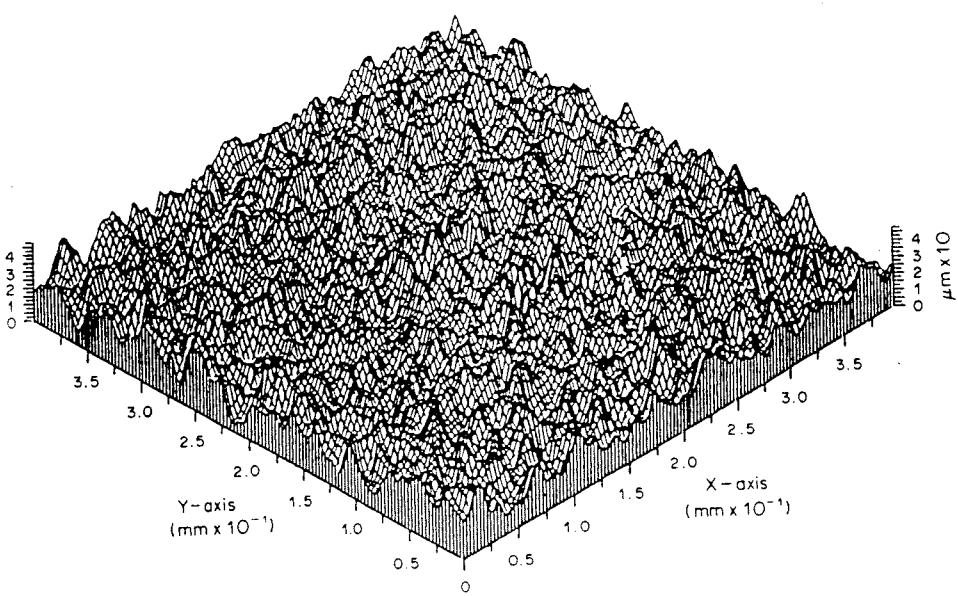


Fig. 4(c). *Caption on p. 524.*

The details of the peening parameters utilized in this study are given in Table 1. The desired peening coverages were obtained by varying the treatment exposure time.

A major problem frequently met in the peening industry is how to measure peening coverage in a component. In practice, the process users resort to the use of 5- and 10-power magnifying glass and/or Dyescan tracers. These *ad hoc* techniques are subjective rather than objective, since they depend entirely upon the judgement and experience of the engineer performing the treatment.

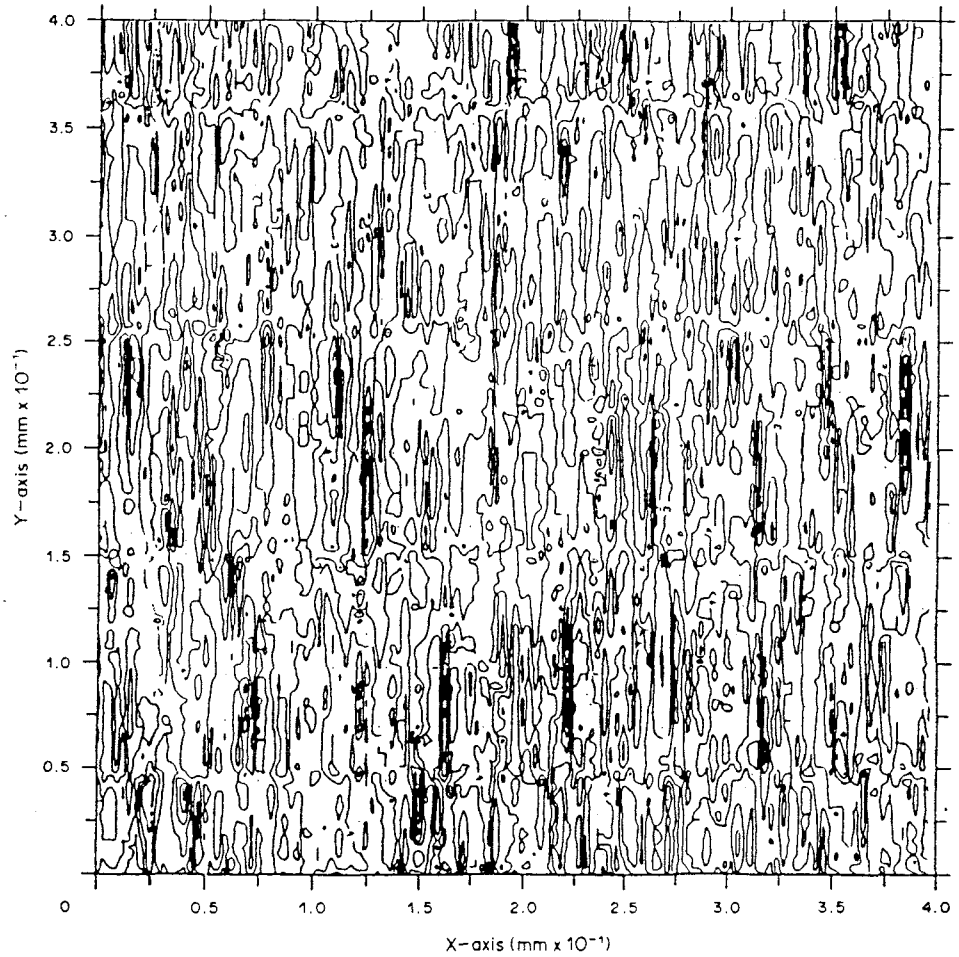


Fig. 4(d). *Caption on p. 524.*

The present study utilizes two complementary techniques to enable the accurate determination of peening coverage. In the first, three dimensional surface roughness measurements were used to correlate peening coverage to surface conditions. In this case, the surface is mapped by making a number of closely-spaced profile traces using a modified stylus-type instrument. Such a technique, however, requires large data handling capabilities, now readily available using mini- or micro-computers, so enabling the surface zone of interest to be scanned and a three-dimensional surface description produced. Figure 4(a) to (c) show typical isometric plots of the ground surface and the different peening coverages examined, while Fig. 4(d) to (f) show contour representation of the projections of the same surfaces.

In the second, the measurements were made using an image and area analyzer. Image and area analyzers primarily use television-type scanners. In this case, the image of the peened surface is formed on the t.v. scanner by an optical microscope, and a video signal is produced. The inherent light integration of the scan tubes give bright, flicker-free images with good signal/noise ratio. The

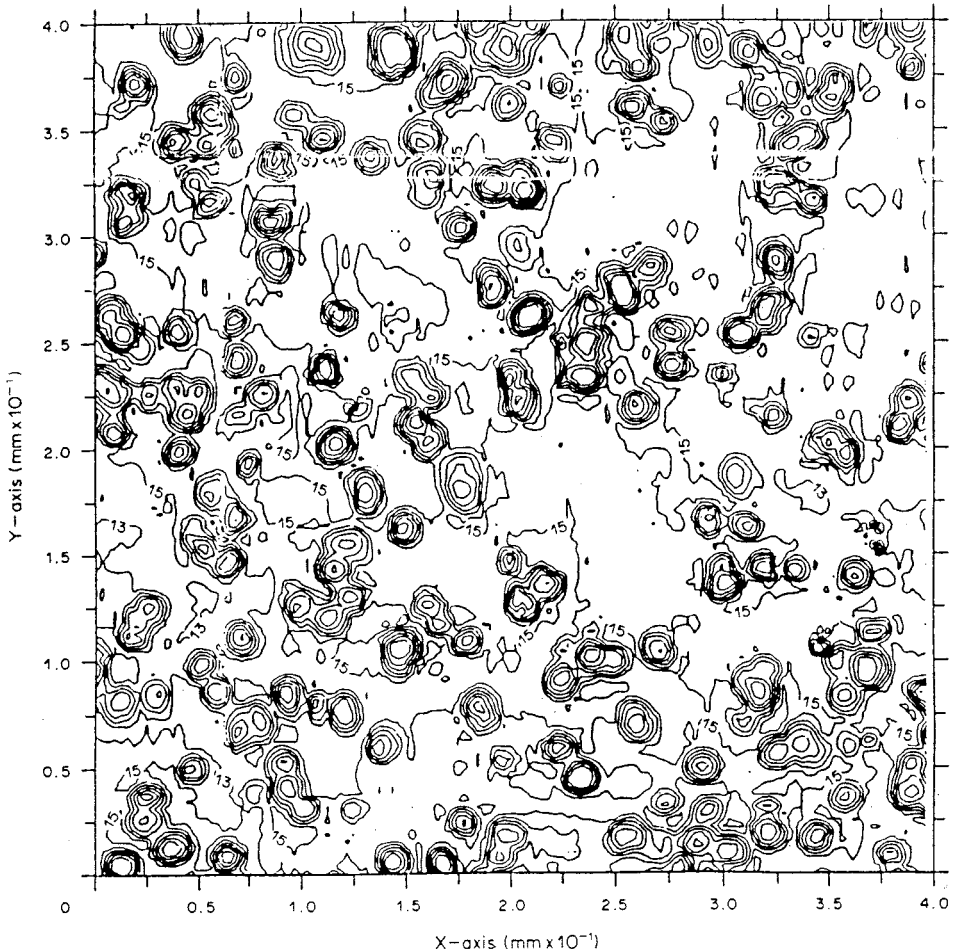


Fig. 4(e). *Caption on p. 524.*

processes which are performed on the signal include a grey level threshold to select the interesting parts of the image, giving a new binary signal corresponding to the wanted and unwanted parts of the picture. This signal passes into special high-speed hardware which produces the required geometrical information. In this case, the image contrast between peened and un-peened areas enables the determination of the peening coverage using this system.

The work was extended to account for the effect of partial-coverage upon the resulting residual stress field using the dissection method [15]. Simple rectangular thin-plate specimens were as being the most suitable for the residual stress measurements. Moreover, it was red sufficiently accurate to base the theory of residual stresses in such specimens on the ce of longitudinal stress only, thus ignoring the true biaxial state of stress which actually exists, and to abide by the assumptions and limitations of the simple beam theory in its development. For the large unidirectional radii of curvatures encountered in the current studies, the above assumptions do not introduce much errors in the determination of the residual stress field.

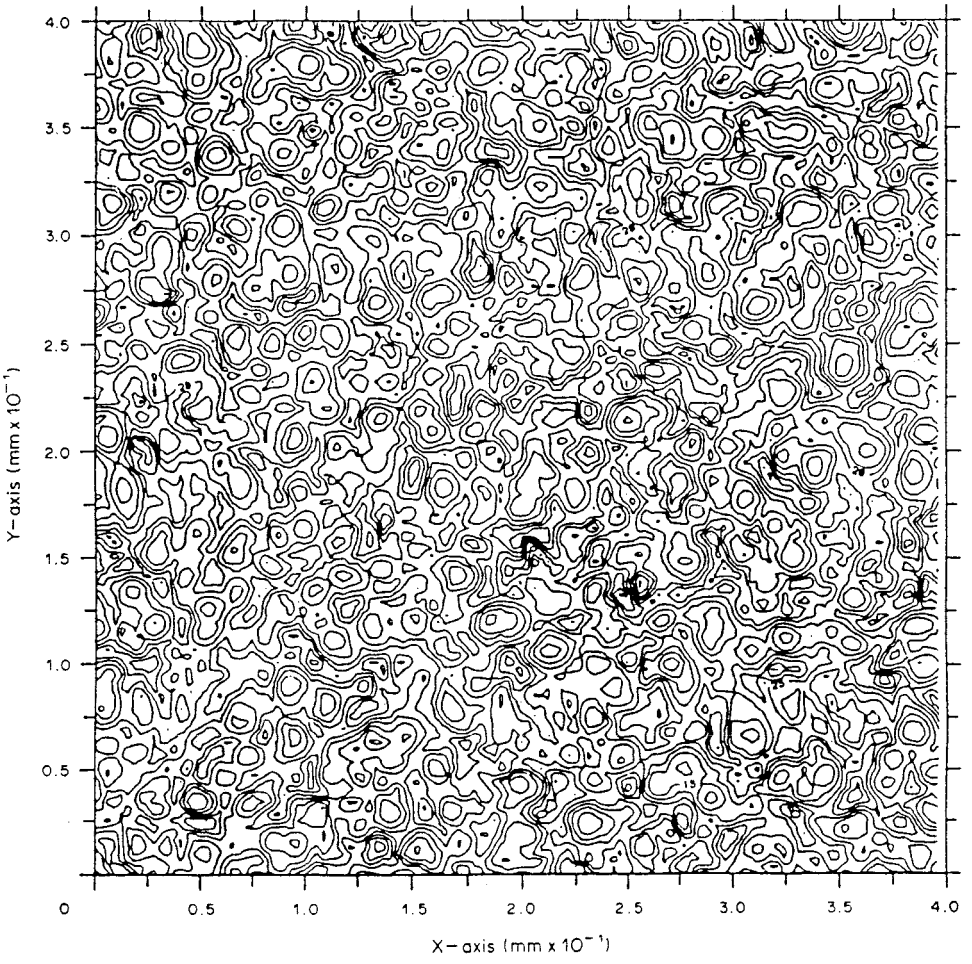


Fig. 4(f)

Fig. 4. Isometric views and contour representations of the steel surfaces examined: (a) a ground surface; (b) partial-coverage of 35%; (c) full-coverage; (d) contour representation of a ground surface; (e) contour representation showing 35% coverage, and (f) contour representation showing full-coverage.

Applying the above theory, one is able to obtain the following expression for the longitudinal residual stress $\sigma^r$ in a specimen of unit width in terms of specimen curvature $\rho$ and thickness

$$\sigma^r = \frac{Et^2}{6}\frac{d\rho}{dt} - \frac{Et}{2}(\rho_0 - \rho) - \frac{1}{t}\int_t^{t_0} \sigma^r \, dt \tag{10}$$

where $E$ is the modulus of elasticity of the specimen's material and $\rho_0$ and $t_0$ are constants defining the original specimen curvature and thickness, respectively.

The curvature as a function of thickness can be defined experimentally by removing thin layers of material from the surface of the specimen in successive stages and the distribution of the longitudinal residual stresses $\sigma^r$ can then be calculated.

The problem of removing uniform, thin layers of surface materials without affecting the residual stresses under consideration is the chief experimental problem involved in the application of the dissection method. Accordingly, chemical machining was adopted throughout the residual stress experiments. The specimen thickness was measured in six places with a high resolution micrometer, and the average of these six measurements was used for the plot of thickness versus curvature. The maximum deviation from the mean seldom amounted to more than 0.01 mm. The curvature measurements were made using an accurate dial gauge arrangement with a resolution of less than 0.005 mm.

## ANALYSIS OF RESULTS AND DISCUSSIONS

The experimental investigation consisted of two main test programmes. The first involved the determination of $\sigma_a$ vs $N$ curves for the different specimens with the view of establishing the fatigue life due to partial peening for varying applied alternating stress, $\sigma_a$. The second involved the development of fatigue crack growth rate data for the investigated materials.

Figure 5 shows the percentage fatigue life improvement for the treated specimens at two different alternating stress levels. At these selected test loads, the fatigue life achieved by the fully-peened specimens is 260% of that achieved by the un-peened specimens, i.e. an improvement of 160%. This improvement is considered modest and is attributed to the relatively high alternating stress $\sigma_a$ used. Another contributing factor to this modest improvement is due to the use of completely reversed bending with $R = -1$; the residual stress field tends to fade out more rapidly with increasing number of cycles. Similar trends were observed for the aluminium specimens (minimum

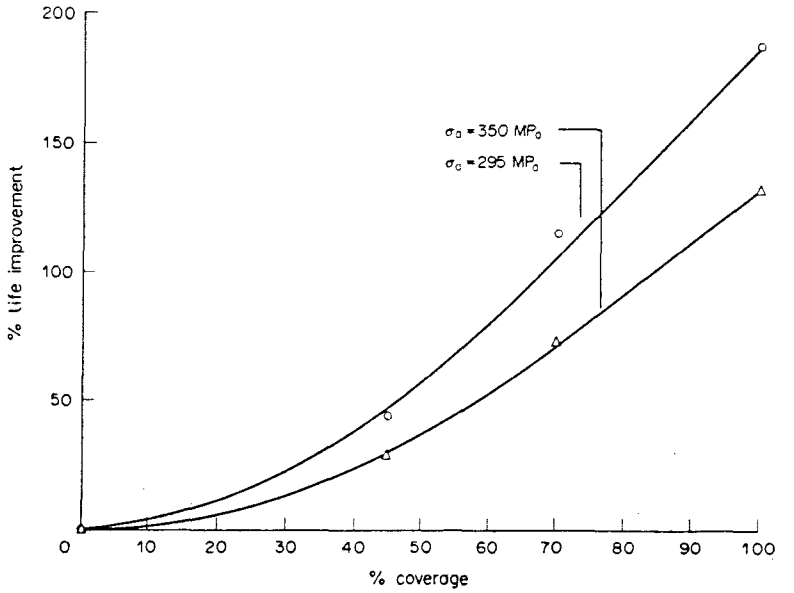


Fig. 5. Fatigue life improvement achieved by fully and partially-peened specimens over that achieved by un-peened specimens at two different stress levels for medium carbon steel specimen.

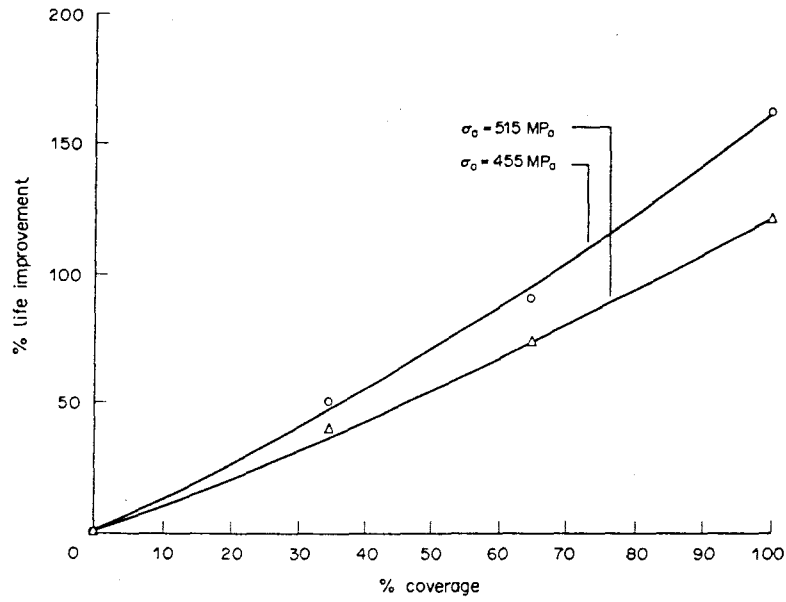


Fig. 6. Fatigue life improvement achieved by fully and partially-peened specimens over that achieved by un-peened specimens at two different stress levels for aluminium specimens.

coverage 45%) and the fatigue life improvement for the different partially and fully-peened specimens are shown in Fig. 6 and the results are summarized in Table 2(b).

Since the fatigue life improvement due to the peening treatment is predominantly governed by the magnitude and the gradient of the compressive residual stress field present in the treated components, it was thought desirable to compare the residual stress fields for the different coverage examined using the previously described dissection method. Figure 7 shows that there exists an axial compressive residual stress field near the exposed surface layers even at the lowest coverage. At this stage, it is important to differentiate between "plastic sub-surface coverage" and "visual

Table 2. Fatigue life improvement achieved by fully and partially-peened specimens over that achieved by un-peened specimens at two different stress levels for:

(a) Medium carbon steel (En 8)

| Peening coverage (%)† | Fatigue life improvement (%) | |
|---|---|---|
| | $\sigma_a$ = 455 MPa | $\sigma_a$ = 515 MPa |
| 35 | 50 | 40 |
| 65 | 90 | 70 |
| 100 | 160 | 120 |

†As measured by image analyzer and surface profilometer.

(b) Aluminium alloy (7075-T6)

| Peening coverage (%)† | Fatigue life improvement (%) | |
|---|---|---|
| | $\sigma_a$ = 295 MPa | $\sigma_a$ = 350 MPa |
| 45 | 45 | 30 |
| 70 | 115 | 75 |
| 100 | 190 | 130 |

†As measured by image analyzer and surface profilometer.

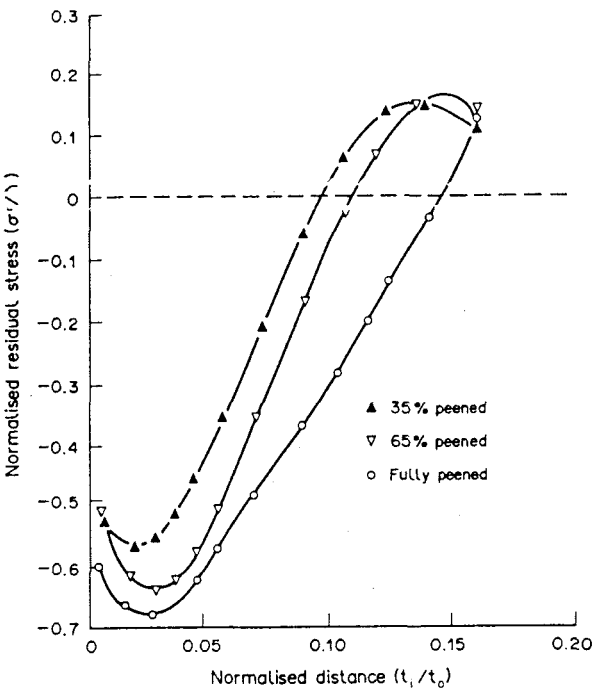


Fig. 7. Axial residual stresses associated with different peening coverage for steel specimens using the dissection method.

surface coverage". Earlier etching work by the author and his collaborators [16] shows that the plastic zone associated with a dent for relatively soft materials is several times (4–5) greater than the size of that dent. Accordingly, while visual inspection of the surface may indicate lack of coverage, sub-surface examination of the plastic zone could reveal complete coverage. This indeed is the main reason for the fatigue life improvement in cases involving partial coverage.

Let us examine the peening treatment of high strength alloys. If one considers the case where the size of the plastic dent is the same as that developed in softer materials, then the size of the plastic zone associated with the increased kinetic energy of the jet stream is again (4–5) times the size of the dent. If on the other hand one utilizes the same kinetic energy as that used in treating relatively softer materials, then a smaller size indentation and accompanying plastic zone will develop. According to plasticity theory for rate-independent materials, the depth of the plastic zone will again remain greater than the reduced size of indentation.

Figure 8(a) shows the crack depth $a$ vs the number of cycles $N$ for fully, partially and un-peened specimens. Two important aspects of this diagram are noticed: (i) peening affects the initiation stage (cracks less than 0.05 mm were considered at the initiation stage) and (ii) reduces the rate at which cracks grow. This was in evidence for both partially and fully-peened specimens. Figure 8(b) shows a trend to that observed above but for the 7075 aluminium specimens. These figures also indicate that initially the crack growth is very slow. This continues until the crack depth reaches a certain value beyond which it accelerates rapidly leading to the final fracture. This implies that peening influences both the initiation and early stages of propagation of fatigue failure. However, once a crack reaches a certain size, then the effect of residual stresses upon fatigue life is greatly reduced.

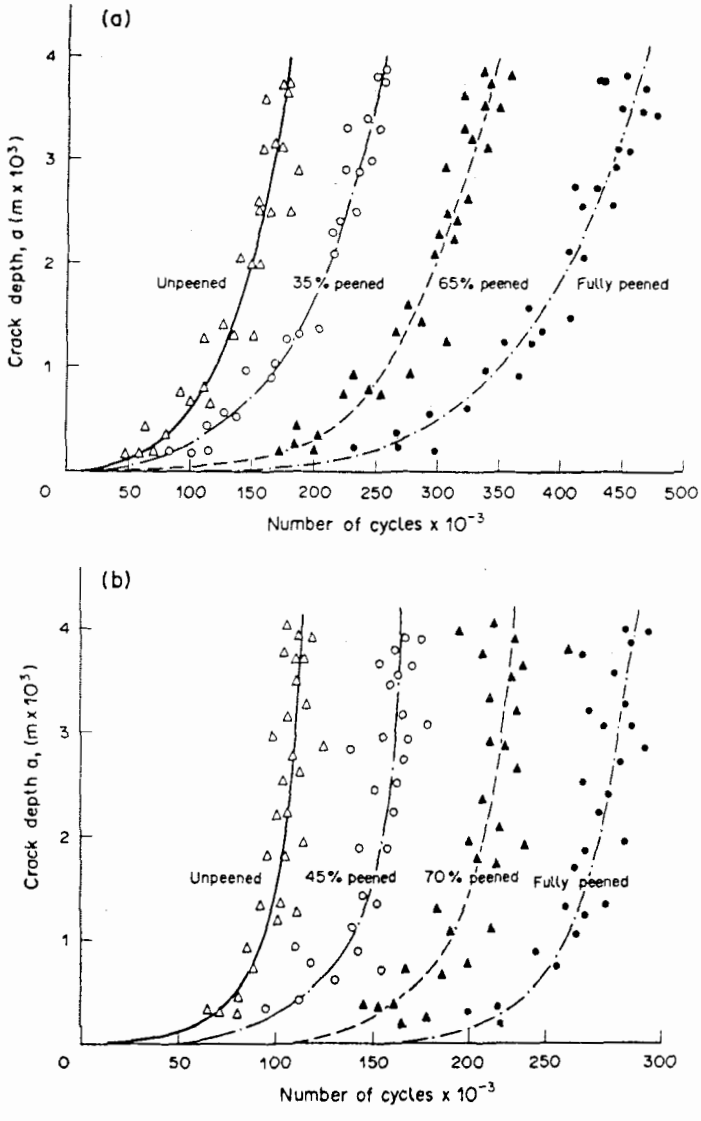


Fig. 8. Semi-crack depth $a$ vs fatigue life $N$ for fully, partially and unpeened: (a) medium carbon steel (En 8) specimens and (b) aluminium alloy (7075) specimens.

The crack depth $a$ vs the number of cycles $N$ relationship was then used, in association with the previously described three-dimensional finite element work, to determine the fatigue crack growth rate relationship. However, no clear indication of trends was observed in the resulting Fig. 9(a) and (b). This may be due to the fact that these figures have not been corrected to account for the effect of residual stresses upon the effective stress intensity factor present in the component. This was complicated by the varying nature of the residual stress field with crack growth, its relaxation with cyclic loading and the continuous measurement of that field. Furthermore, no account was taken of complete and partial-contacts of the cracked surfaces in the compressive side of the specimens upon $K_I$ nor of the anomalous behaviour of short cracks. As a result of these difficulties, Fig. 9(a) and (b) must be viewed with caution.

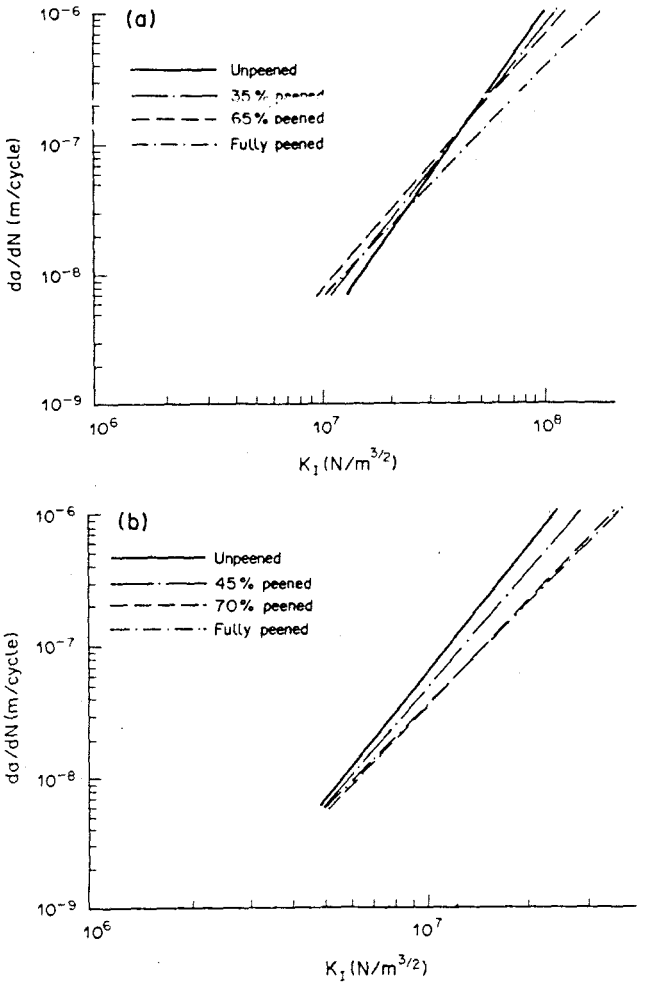


Fig. 9. Fatigue crack growth rate curves for fully, partially and un-peened: (a) medium carbon steel specimens (En 8) and (b) aluminium alloy specimens.

## CONCLUSIONS

The objective of this study has been to evaluate whether partial-peening coverage is detrimental to the fatigue performance of the treated components. It was also desired to determine whether any life improvement can be achieved by this partial peening treatment.

Both fully-peened and partially-peened En 8 medium carbon steel (minimum coverage 35%) and 7075 aluminium alloy (minimum coverage 45%) specimens yielded an improvement in their fatigue lives over their respective un-peened specimens. For example, for the steel specimens an improvement of approximately 50% was observed for 35% coverage and 90% for 65% coverage in comparison with 160% fully-covered specimens at a stress level of 456 MPa. Similar trends were observed for the 7075 aluminium trials.

In spite of the scatter inherent in all fatigue testing, this investigation consistently showed that the present partial-peening treatment is not detrimental to the fatigue performance of the studied materials. It also showed that fully-peened specimens attain superior life improvement from the

treatment. The improved fatigue life associated with partial-coverage has been attributed to what is termed in this study as "plastic coverage" experienced by the component at the sub-surface level.

*Acknowledgements*—The author gratefully acknowledges the financial support provided by Natural Sciences and Engineering Research Council of Canada.

## REFERENCES

1. S. A. Meguid (1989) Shot-peening and peen-forming; Theory and application. Short Course Notes, University of Toronto, Toronto.
2. S. A. Meguid (1975) The mechanics of the shot-peening process. Ph.D. thesis, U.M.I.S.T., England.
3. S. A. Meguid (1983) Troubles caused by metal fatigue and engineering interests in compressive residual stresses. Presented at *First Int. Conf. on Impact Treatment Processes*, Cranfield.
4. A. E. Green and I. M. Sneddon (1950) The distribution of stress in the neighborhood of a fault elliptical crack in an elastic solid. *Proc. Cambr. Phil. Soc.* **47**, 159–164.
5. M. K. Kassir and G. C. Sih (1966) Three-dimensional stress distribution around an elliptical crack under arbitrary loadings. *J. appl. Mech.* **88**, 601–611.
6. R. C. Shan and A. S. Kobayashi (1971) Stress-intensity factor for an elliptical crack around arbitrary normal loading. *Engng Fract. Mech.* **3**, 71–96.
7. K. Vijayakumar and S. N. Atluri (1981) An embedded elliptical flaw in an infinite solid subject to arbitrary crack-face tractions. *Trans. ASME J. appl. Mech.* **48**, 88–96.
8. G. C. Sih and H. Liebowitz (1968) Mathematical theories of brittle fracture. In *Fracture II*. Academic Press, New York.
9. J. P. Benthem and W. T. Koiter (1973) Asymptotic approximations to crack problems. In *Methods of Analysis and Solutions of Crack Problems* (Edited by G. C. Sih), Chap. 3, pp. 131–178. Noordhoft, Gröningen, Holland.
10. D. O. Harris (1967) Stress intensity factors for hollow circumferentially notched round bars. *J. Basic Engng* **89**, 49–54.
11. S. A. Meguid (1989) *Engineering Fracture Mechanics*. Elsevier Applied Science, London.
12. Annual Book of ASTM Standard, Fatigue testing and the statistical analysis of fatigue data (1986) Metals-Mechanical Testing; Elevated and Low-Temperature Tests. ASTM: **E206-72**, pp. 363–369.
13. British Standards Institution (1962) Methods of fatigue testing: Rotating bending fatigue tests. BS 8, Part 2.
14. W. D. Dover, F. D. W. Charlesworth, K. A. Taylor, R. Collins and D. H. Michael (1981) The use of A.C. field measurements to determine the shape and size of a crack in a metal. Eddy-current characterization of materials and structures (Edited by G. Birnbaum and G. Free). ASTM STP 722, pp. 401–427.
15. G. Sachs and G. Espey (1941) The measurement of residual stresses in metal. *The Iron Age*, Slept. 18, pp. 36–42 and Sept. 25, pp. 36–42.
16. S. A. Meguid and M. S. Klair (1985) An examination of the relevance of co-indentation studies to incomplete coverage in shot-peening using the finite-element method. *J. Mech. Working Tech.* **11**, 87–104.